Implications of Gnomonic Distortion on Electron Backscatter Diffraction and Transmission Kikuchi Diffraction

Chris M. Fancher,[1] Matthew J. Burch,[2] Srikanth Patala,[2] and Elizabeth C. Dickey[3]

[1] Material Science and Technology Directorate, Oak Ridge National Laboratory, 1 Bethel Valley Road, Oak Ridge, TN 37831, USA

[2] Department of Materials Science and Engineering, North Carolina State University, Raleigh, NC, 27695, USA

[3]Department of Materials Science and Engineering, Carnegie Mellon University, Pittsburgh, PA 15213, USA

This article has been accepted for publication and undergone full peer review but has not been through the copyediting, typesetting, pagination and proofreading process, which may lead to differences between this version and the Version of Record. Please cite this article as doi: 10.1111/jmi.13077.

access to these results of federally sponsored research in accordance with the DOE Public Access Plan (http://energy.gov/downloads/doe-public-access-plan).

Abstract

The effect of gnomonic distortion on orientation indexing of electron backscatter diffraction patterns is explored through simulation of electron diffraction patterns for sample-to-detector geometries associated with transmission Kikuchi diffraction (TKD) and electron backscatter diffraction (EBSD). Simulated data were analyzed by computing a similarity index for both Hough transformed data and simulated patterns to determine the sensitivity of each method for detecting subtle differences in the effect of gnomonic distortions on electron diffraction patterns. These results indicate that the increased gnomonic distortions in electron diffraction patterns for a TKD geometry enhance the sensitivity for detecting subtle differences in interband angles. Additionally, the utilization of a Hough transform based indexing approach further enhances the sensitivity.

Abstract

Electron backscatter diffraction (EBSD) and transmission Kikuchi diffraction (TKD) have become vital tools for studying materials. These probes provide information about how locally arranged. EBSD and TKD utilize different experimental configurations that have

impacts the measured data. The projection of the electron diffraction Ewald's sphere onto the face of the detectors results in Gnomonic distortions, and the selection of experimental configuration affects the magnitude of these distortions. In this work we used simulated dynamical electron diffraction patterns (EDPs) to understand the how differences in the EBSD and TKD experimental configurations impacts Gnomonic distortions and how these distortions effect the sensitivity of each method for detecting subtle differences in interband angles. These results indicate that the increased gnomonic distortions in electron diffraction patterns for a TKD geometry enhance the sensitivity for detecting subtle differences in interband angles. These results also suggest that a traditional Hough transform approach for indexing EDP data is less sensitive to detecting slight deviations than direct analysis of EDPs.

Introduction:

Electron backscatter diffraction (EBSD) has become a vital characterization technique for orientation analysis of crystalline materials.[1] In addition to EBSD, the relatively new

method of transmission Kikuchi diffraction (TKD) provides identical information as traditional EBSD. The transmission setup enables TKD to achieve a superior spatial resolution (~5 nm).[2,3] Orientation information is extracted from EBSD and TKD indexing algorithms that utilize the Hough transform, which is a transformation designed to identify lines in an image through the parametric equation:

$$\rho = x\cos\theta + y\sin\theta \quad \textbf{(1)}$$

where ρ is the shortest distance between the origin (generally the center of the pattern) and the band and θ is the angle between the x-axis and the perpendicular line from the origin.[4] Care must be taken to discretize ρ-θ, for example, obtaining a unique solution requires θ space be restricted to the interval [0, π). [5] Selecting an unapproached discretization or interval can have adverse effects on the transformation. Performing a Hough transform on two-dimensional patterns transforms the information into ρ-θ space, where lines are transformed into points. These points are then identified using a butterfly mask. The angles between the points in Hough space are computed and compared to a table of simulated orientations for the input material.[6]

Both EBSD and TKD use a Hough transform-based orientation indexing method that is only sensitive to detecting differences in interband angles of ~0.5 degrees.[7] That is, the Hough transform-based indexing cannot differentiate between distinct orientations that have interband angles below this tolerance. Winkelmann *et al.* recently presented a new high-precision orientation refinement using simulated reference patterns that achieves 0.03° resolution.[8] High-resolution EBSD (HR-EBSD) methods utilize cross-correlation to identify subtle angular differences in diffraction patterns to extract strain and orientation

information that improves the maximum angular resolution to as small as 0.01°.[9,10] HR-EBSD requires either a strain-free pattern for comparison or a simulated reference of the strain-free material for the specific zone axis of interest.[11–15] Advances in digital image correlations methods have improved HR-EBSD and HR-TKD techniques.[16–18]

Dictionary indexing (DI) offers an alternative approach for indexing electron diffraction patterns.[19,20] Instead of identifying the maximum in a transformed dataset, the DI method directly operates on the measured data through a *normalized inner-product* of the pattern of interest and a dictionary of simulated reference patterns. While the technique does not directly improve the indexing capabilities, the DI method can index patterns containing overlapping diffraction patterns and is less sensitive to noise in experimental patterns.[19,21] The subsequent gains in indexing sensitivity come with a substantial computational expense that can limit the maximum achievable angular resolution.[22] Improving the indexing sensitivity of DI requires a fine degree of cubochoric coverage.[21] A spherical harmonic alternative was developed that achieves similar indexing sensitivity with a lower computational expense.[23]

The geometric differences in the experimental setup between EBSD and TKD are shown in Figure 1. The working distance for EBSD is typically set to minimize the distance between the sample and the EBSD detector, which for many systems is ~5-15 mm, with the pattern center (PC) lying near the center of the detector.[24,25] The PC is defined as the intersection of the plane of the EBSD detector with a sphere where the radius is the shortest distance between the Ewald's sphere and detector surface. In contrast, a shorter working distance (2-4 mm) is commonly used in TKD to maximize signal incident upon the

detector.[2,26,27] The change in working distance shifts the PC, as is illustrated in Figure 1. The combined effect of a shift in PC and increased sample-to-detector distance impacts the angular range of the Kikuchi diffraction sphere incident on the detector and subsequent gnomonic projection of the Ewald's sphere onto the detector surface. In a gnomonic projection, a point on the Ewald's sphere is projected onto the plane of the EBSD detector by a ray that originates at the center of the sphere. A gnomonic projection distorts Kikuchi bands from slightly hyperbolic into more parabolic traces in the electron diffraction pattern (EDP). Advances with 3-dimensional Hough transforms account for the non-linear deviations (hyperbolic and parabolic) to improve orientation imaging.[28,29]

In this work, we simulate dynamical EDPs to determine the effect of gnomonic distortions on the sensitivity of Hough and dictionary-based indexing methods to identify subtle lattice distortions. These results demonstrate that gnomonic distortions, exaggerated for short working distances, can improve sensitivity for identifying subtle differences between orientations with similar interband angles. Furthermore, these results also suggest that gnomonic distortions are exaggerated by Hough transforms.

Simulation and Analysis Procedure

For simplicity, the working distance for the electron diffraction is herein referred to as EBSD geometry, i.e., a backscattering geometry with the pattern center near the center of the detector, and TKD geometry, in a forward scatter geometry with the pattern center far above the detector. A 70° sample tilt relative to the incident electron beam direction was used for both the TKD and EBSD geometries to isolate the effects of working distance. Dynamical

EDP for an aluminum sample with a hypothetical tetragonal distortion (c/a of 1.0-1.025) was generated using EMsoft (v 4.0).[19] Electron diffraction patterns were simulated for the tetragonal distortion along the [100], [010], and [001] directions for 1000 random combinations of Bunge Euler angles in the interval ($0\leq\phi_1\leq360$, $0\leq\Phi\leq90$, $0\leq\phi_2\leq90$). The effect of differences in the simulated diffraction data for a distortion oriented along the [100], [010], and [001] directions are compared in Figure 2. Specifics of the working distance are not a direct input into EMsoft (e.g., 10.2, 7.0, etc.); instead, differences in the working distance are manifested as changes in sample-to-detector distance and PC. The EBSD PC and sample-to-detector were initially determined by optimizing these parameters for a 10mm distance using an Oxford ferritic standard. Changes to the sample-to-detector distance and PC for a 2mm working distance were determined geometrically.

The effect of gnomonic distortions was quantified by calculating the *normalized inner-product* between a deformed and undeformed reference:

$$\rho_i = \langle \frac{P_l}{\|P_l\|} \cdot \frac{R}{\|R\|} \rangle \quad \textbf{(2)}$$

Where P_l and R represent the vectorized patterns for the reference and rotated pattern.[21] This *normalized inner-product* was determined for both 1) simulated and 2) Hough transformed data. Hough transforms were generated by first identifying line edges using the Canny filter in skimage.feature. Filtered data were transformed using the skimage.transform hough_line algorithm.[30] Simulated diffraction data for the EBSD and TKD geometries were analyzed using a common set of Canny filtering and Hough transform inputs. Figure 3 compares each step of the Hough transform process for noise-free EBSD and TKD data,

respectively. This study uses the entire EDP to determine the effect of the experimental setup on the gnomonic distortions.

Results and Discussion:

It should be reiterated that the only difference in simulated patterns for the EBSD and TKD settings is a change in PC with respect to the detector and the consequent changes in the projection of the diffraction sphere onto the detector. In the EBSD setting, the diffraction sphere originating from the sample is projected onto the EBSD detector, as shown in Figure 1. In Figure 4, the z-axis is along the vector joining the sample and pattern center on the detector. This projection can be described with the transformation equations described below:

$$(R, \Phi) = (r\tan(\theta), \phi) \quad \textbf{(3)}$$

$$(X, Y) = (r\tan(\theta)\cos(\phi), r\tan(\theta)\sin(\phi))$$

where θ and ϕ are the polar, and the azimuthal angles, respectively, and r is the distance between the sample and the PC, as shown in Figure 4.

In a gnomonic projection, great circles are mapped from the sphere onto a two-dimensional plane (*e.g.,* electron diffraction detector face). One consequence of the gnomonic projection is demonstrated in Figure 4, where equidistant points on the diffraction sphere are projected to non-equidistant points on the detector face. Utilizing the close working distance used in the TKD geometry shifts the PC closer to the pole piece or higher on the detector face, which increases the angle θ for regions of the detector and enhances gnomonic distortions, even at the center of the detector. Other consequences of the gnomonic projection in EBSD are the loss in intensity of the Kikuchi patterns, and an increase in the bandwidth as

the polar angle θ is increased. The loss of intensity incident on the detector is a reason why gnomonic distortions are typically regarded as being undesirable for the indexing of EBSD patterns.[31] Small working distances are generally used in TKD to optimize spatial resolution and pattern intensity.[27] This decreased working distance increases the distance between the sample and detector. The increased sample detector distance could degrade pattern intensity in EBSD data. However, in TKD, the intensities and the quality of the projected Kikuchi pattern remain excellent despite the longer sample-detector distance.[2,26]

As a thought experiment, which demonstrates how gnomonic projection impacts orientation analysis, the reader can imagine obtaining an EBSD map within a single grain. If the orientation (Euler angle) of this grain is then perturbed slightly (± 2°), the position of the zone axis within the EBSD/TKD pattern (i.e., the point where multiple Kikuchi bands intersect) is also perturbed. The technique's sensitivity depends on how small the differences between two patterns can be confidently distinguished by the indexing method. From the equations above, it can be shown that a perturbation (i.e., $ds = \sqrt{d\theta^2 + d\phi^2}$) of the zone-axis on a unit sphere is related to the change in its position (dR) on the detector as:

$$\frac{dR}{ds} = r \sec^2 \theta \quad \textbf{(4)}$$

Therefore, the perturbation is magnified by the distance of the PC from the sample (by a factor of r) and polar angle (through $\sec^2 \theta$). In the TKD setting, both r and θ are increased. This increase in r and θ results in a more significant distortion, which improves the sensitivity of band indexing. This effect can be magnified with larger values of R and θ; however, Nowell and Wright demonstrated a limit on how far the detector can be moved

farther away before the loss of intensity and degradation in pattern quality would prevent indexing.[32]

The sensitivity to detect differences in gnomonic distortions on EDP was assessed by determining the normalized inner-product between the vectorized simulated dataset for a random orientation and the analogous orientation representing a 90° rotation about the x-, y-, or z-axis.[21] The *normalized inner-product* was performed using both raw diffraction and Hough transformed data to understand the impact of the Hough transform on gnomonic distortions for a tetragonal distortion along the [100], [010], and [001] directions. Figure 5 compares the correlation index as a function of tetragonal distortion. A correlation index of less than one is found for all datasets with a c/a -1 > 0, indicating that a 90° rotation about the [100], [010], and [001] directions are distinguishable. The correlation index of the Hough transformed, and diffraction data has very different dependencies on c/a. A nearly linear reduction in the correlation is observed in diffraction space, while the index initially reduces quickly before more slowly decreasing for the Hough transformed data. The lower correlation index for the Hough transformed TKD setting data suggests that distinct orientations are more easily distinguished.

These data indicate that gnomonic distortions due to a change in the PC (EBSD vs. TKD) have less impact on the correlation index for diffraction data than after a Hough transform. Diffraction data showed no difference for the TKD and EBSD settings. In contrast, the lower correlation for the TKD after performing a Hough transform indicates that the underlying transformation from diffraction to Hough space magnifies differences in the angular distortion. From Eqn. 4, the effect of gnomonic distortions is related to the sample to

PC and the angular range from the PC to a given point on the detector surface. Observing no difference in the correlation for the TKD and EBSD geometries in the diffraction data indicate that, while present, the difference in the gnomonic distortions is subtle. However, the transformation into Hough space magnifies the subtle (potentially pixel or subpixel shifts), making the differences detectable. Since the correlation of the TKD-based geometry is lower than the EBSD-based geometry for all c/a ratios greater than 1, this result demonstrates that the differences between two patterns with a 90°-unit cell rotation difference are enhanced in the TKD based geometry.

Fully exploring the impact of gnomonic distortions requires the consideration of how noise level affects each analysis method. Varying levels of salt and pepper noise were introduced to the simulated data to determine how noise in measured diffraction data impacts the effect of gnomonic distortions, with the signal-to-noise being determined by:

$$SNR = 10\log_{10}\left(\frac{{I_{\max}}^2}{MSE}\right) \quad \textbf{(4)}$$

where MSE is the mean squared error between the simulated pattern and pattern with added noise. See Figure 6 for a comparison of a representative EDP with differing levels of noise and the effect of noise on the line detection in the simulated data. Random noise in the low signal-to-noise data significantly impacts line detection, where the initially smooth lines detected from the Canny filtering become wavy at low SNR. This underlying randomness has been shown to prohibit the use of the Hough-transform-based indexing approach. However, these noisy data are still suitable for the dictionary indexing method.[21]

Increased noise level adversely impacts all correlation indexes, with the analysis of raw diffraction data showing a constant reduction with noise (see Figure 7). The Hough transform analysis initially show a decrease in correlation index before increasing. We note that the TKD geometry maintains a lower correlation up to 28.63 SNR. Higher noise causes the Hough transform to break down at high noise and would not detect lines leading to an empty or nearly empty ρ-θ space (leading to more similarity than differences). An increase at the highest noise level indicates that sufficient noise was introduced to cause a breakdown of the Hough transform, preventing the detection of Kikuchi lines. While noise negatively impacts the efficacy of the Hough transforms for detecting lines, these data indicate that the TKD setting consistently achieved a lower correlation index than the EBSD setting. This result suggests that gnomonic distortions could lead to higher confidence when indexing the two distinct orientations. It should be noted that the shifting of the PC and subsequent increase in the sample-to-detector distance can increase the noise in the measured diffraction data.

Gnomonic distortions are nearly ubiquitous in all EBSD setups, and it is helpful to understand how these distortions affect indexing confidence. This is especially true as EBSD detector configurations are designed to reduce or remove gnomonic distortion from EBSD patterns.[33,34] For the TKD setting, where high gnomonic distortions can be achieved without the loss of diffraction intensity, the increased sensitivity to identify distortions may be applied to several different applications. One specific example is the imaging of ferroelastic domains in ferroelectric oxides. The lattice distortion of many tetragonal

ferroelectric oxides is less than 1.02, making the determination of 90° domain structures difficult using traditional Hough-based indexing of EBSD data. A subtle deviation in c/a from one complicates orientation indexing because slight distortions only give rise to a subtle difference in indexing confidence.[32] The results presented in this work suggest that utilizing a working distance that enhances gnomonic distortions is a potential avenue to more readily discriminate between the differently oriented domain in material with subtle lattice distortions and twins.[35] Alternatively, the use of a lower accelerating voltage results in an EDP with wider Kikuchi bands that would similarly enhance the impact of gnomonic distortions with the added benefit of improving spatial resolution.[36] It should be noted that this would not be true for 180° domain variants in ferroelectrics, as Hough transform-based indexing is insensitive to inversion symmetry. Instead, fine structure in electron diffraction patterns must be analyzed against dynamically simulated reference patterns to determine the chirality of the material.[37,38]

Conclusion

Results presented in this paper indicate that gnomonic distortions could enhance sensitivity for detecting subtle differences in interband angles. The effect of gnomonic distortions on the EDPs can be tuned through the use of different sample-to-detector settings, e.g., an EBSD or TKD experimental condition that shifts the PC closer to the pole piece and increases the gnomonic projection angle θ, or by reducing accelerating voltage. The effects associated with gnomonic distortions are more prominent in data that were filtered and treated with a Hough-transform, even with moderate noise in the EDPs. EDPs analyzed in diffraction

space, *i.e.*, raw patterns, exhibit a more minor difference in the normalized inner-product correlation index than Hough space, filtered and treated with a Hough-transform. The differences in the results between Hough and diffraction space are attributed to the magnification of subtle (potentially pixel or subpixel shifts) during the transformation.

Acknowledgments

This material is based upon work supported by the U.S. Department of Energy, Office of Science, Office of Basic Energy Sciences, under contract number DE-AC05-00OR22725. This material is based upon the National Science Foundation work as part of the Center for Dielectrics and Piezoelectrics under Grant Nos. IIP-1361571 and IIP-1361503 and the National Science Foundation Graduate Research Fellowship for M.J. Burch under Grant No. DGE-0946818. Any opinion, findings, conclusions, or recommendations expressed in this material are those of the authors(s) and do not necessarily reflect the views of the National Science Foundation.

References

[1] Wilkinson AJ, Britton T Ben. Strains, planes, and EBSD in materials science. Materials Today 2012;15:366–76. https://doi.org/10.1016/S1369-7021(12)70163-3.

[2] Trimby PW. Orientation mapping of nanostructured materials using transmission Kikuchi diffraction in the scanning electron microscope. Ultramicroscopy 2012;120:16–24. https://doi.org/10.1016/j.ultramic.2012.06.004.

[3] Keller RR, Geiss RH. Transmission EBSD from 10 nm domains in a scanning electron microscope. Journal of Microscopy 2012;245:245–51. https://doi.org/10.1111/j.1365-2818.2011.03566.x.

[4] Dingley DJ, Field DP. Electron backscatter diffraction and orientation imaging microscopy. Materials Science and Technology 1997;13:69–78. https://doi.org/10.1179/mst.1997.13.1.69.

[5] Newman W, Duda RO, Hart PE. Graphics and Use of the Hough Transformation To Detect Lines and Curves in Pictures. n.d.

[6] Wright SI, Nowell MM. EBSD image quality mapping. Microscopy and Microanalysis 2006;12:72–84. https://doi.org/10.1017/S1431927606060090.

[7] Dingley DJ, Field DP. Electron backscatter diffraction and orientation imaging microscopy. Materials Science and Technology 1997;13:69–78. https://doi.org/10.1179/mst.1997.13.1.69.

[8] Winkelmann A, Jablon BM, Tong VS, Trager-Cowan C, Mingard KP. Improving EBSD precision by orientation refinement with full pattern matching. Journal of Microscopy 2020;277:79–92. https://doi.org/10.1111/jmi.12870.

[9] Wilkinson AJ, Meaden G, Dingley DJ. High-resolution elastic strain measurement from electron backscatter diffraction patterns: New levels of sensitivity. Ultramicroscopy 2006;106:307–13. https://doi.org/10.1016/j.ultramic.2005.10.001.

[10] Britton B, Holton I, Meaden G, Dingley D. High angular resolution electron backscatter diffraction : measurement of strain in functional and structural materials. Microscopy and Analysis 2013:1–5.

[11] Burnett TL, Weaver PM, Blackburn JF, Stewart M, Cain MG. Correlation of electron backscatter diffraction and piezoresponse force microscopy for the nanoscale characterization of ferroelectric domains in polycrystalline lead zirconate titanate. Journal of Applied Physics 2010;108:042001. https://doi.org/10.1063/1.3474940.

[12] Howell J a., Vaudin MD, Cook RF. Orientation, stress, and strain in an (001) barium titanate single crystal with 90° lamellar domains determined using electron backscatter diffraction. Journal of Materials Science 2014;49:2213–24. https://doi.org/10.1007/s10853-013-7915-3.

[13] Farooq MU, Villaurrutia R, MacLaren I, Burnett TL, Comyn TP, Bell a. J, et al. Electron backscatter diffraction mapping of herringbone domain structures in tetragonal piezoelectrics. Journal of Applied Physics 2008;104:024111. https://doi.org/10.1063/1.2956704.

[14] Potnis P, Tsou N, Huber J. A Review of Domain Modelling and Domain Imaging Techniques in Ferroelectric Crystals. Materials 2011;4:417–47. https://doi.org/10.3390/ma4020417.

[15] Yang B, Park NJ, Seo BI, Oh YH, Kim SJ, Hong SK, et al. Nanoscale imaging of grain orientations and ferroelectric domains in (Bi1−xLax)4Ti3O12 films for ferroelectric memories. Applied Physics Letters 2005;87:062902. https://doi.org/10.1063/1.2009835.

[16] Ernould C, Beausir B, Fundenberger JJ, Taupin V, Bouzy E. Global DIC approach guided by a cross-correlation based initial guess for HR-EBSD and on-axis HR-TKD. Acta Materialia 2020;191:131–48. https://doi.org/10.1016/j.actamat.2020.03.026.

[17] Ruggles TJ, Bomarito GF, Qiu RL, Hochhalter JD. New levels of high angular resolution EBSD performance via inverse compositional Gauss–Newton based digital image correlation. Ultramicroscopy 2018;195:85–92. https://doi.org/10.1016/j.ultramic.2018.08.020.

[18] Vermeij T, Hoefnagels JPM. A consistent full-field integrated DIC framework for HR-EBSD. Ultramicroscopy 2018;191:44–50. https://doi.org/10.1016/j.ultramic.2018.05.001.

[19] Chen YH, Park SU, Wei D, Newstadt G, Jackson MA, Simmons JP, et al. A Dictionary Approach to Electron Backscatter Diffraction Indexing. Microscopy and Microanalysis 2015;21:739–52. https://doi.org/10.1017/S1431927615000756.

[20] Singh S, De Graef M. Orientation sampling for dictionary-based diffraction pattern indexing methods. Modelling and Simulation in Materials Science and Engineering 2016;24:085013. https://doi.org/10.1088/0965-0393/24/8/085013.

[21] Ram F, Wright S, Singh S, De Graef M. Error analysis of the crystal orientations obtained by the dictionary approach to EBSD indexing. Ultramicroscopy 2017;181:17–26. https://doi.org/10.1016/j.ultramic.2017.04.016.

[22] Singh S, Ram F, De Graef M. Application of forward models to crystal orientation refinement. Journal of Applied Crystallography 2017;50:1664–76. https://doi.org/10.1107/S1600576717014200.

[23] Lenthe WC, Singh S, Graef M De. A spherical harmonic transform approach to the indexing of electron back-scattered diffraction patterns. Ultramicroscopy 2019;207:112841. https://doi.org/10.1016/j.ultramic.2019.112841.

[24] Zeafferer S, Wright SI. Electron Backscatter Diffraction in Materials Science. Boston, MA: Springer US; 2009. https://doi.org/10.1007/978-0-387-88136-2.

[25] Suzuki S. Features of transmission EBSD and its application. JOM 2013;65:1254–63. https://doi.org/10.1007/s11837-013-0700-6.

[26] Trimby PW, Cao Y, Chen Z, Han S, Hemker KJ, Lian J, et al. Characterizing deformed ultrafine-grained and nanocrystalline materials using transmission Kikuchi diffraction in

a scanning electron microscope. Acta Materialia 2014;62:69–80. https://doi.org/10.1016/j.actamat.2013.09.026.

[27] Suzuki S. Features of transmission EBSD and its application. JOM 2013;65:1254–63. https://doi.org/10.1007/s11837-013-0700-6.

[28] Maurice C, Fortunier R. A 3D Hough transform for indexing EBSD and Kossel patterns. Journal of Microscopy 2008;230:520–9. https://doi.org/10.1111/j.1365-2818.2008.02045.x.

[29] Thomsen K, Schmidt NH, Bewick A, Larsen K, Goulden J. Improving the Accuracy of Orientation Measurements using EBSD. Microscopy and Microanalysis 2013;19:724–5. https://doi.org/10.1017/s1431927613005618.

[30] van der Walt S, Schönberger JL, Nunez-Iglesias J, Boulogne F, Warner JD, Yager N, et al. scikit-image: image processing in Python. PeerJ 2014;2:e453. https://doi.org/10.7717/peerj.453.

[31] Nowell MM, Wright SI. Orientation effects on indexing of electron backscatter diffraction patterns. Ultramicroscopy, vol. 103, 2005, p. 41–58. https://doi.org/10.1016/j.ultramic.2004.11.012.

[32] Nowell MM, Wright SI. Orientation effects on indexing of electron backscatter diffraction patterns. Ultramicroscopy, vol. 103, 2005, p. 41–58. https://doi.org/10.1016/j.ultramic.2004.11.012.

[33] Bruker. OPTIMUS™ TKD Detector Head 2016.

[34] Fanta ABS, Fuller A, Alimadadi H, Todeschini M, Goran D, Burrows A. Improving the imaging capability of an on-axis transmission Kikuchi detector. Ultramicroscopy 2019;206:112812. https://doi.org/10.1016/j.ultramic.2019.112812.

[35] Rampton TM, Wright SI, Miles MP, Homer ER, Wagoner RH, Fullwood DT. Improved twin detection via tracking of individual Kikuchi band intensity of EBSD patterns. Ultramicroscopy 2018;185:5–14. https://doi.org/10.1016/j.ultramic.2017.11.003.

[36] Steinmetz DR, Zaefferer S. Towards ultrahigh resolution EBSD by low accelerating voltage. Materials Science and Technology 2010;26:640–5. https://doi.org/10.1179/026708309X12506933873828.

[37] Winkelmann A, Nolze G. Chirality determination of quartz crystals using Electron Backscatter Diffraction. Ultramicroscopy 2015;149:58–63. https://doi.org/10.1016/j.ultramic.2014.11.013.

[38] Burch MJ, Fancher CM, Patala S, De Graef M, Dickey EC. Mapping 180° polar domains using electron backscatter diffraction and dynamical scattering simulations. Ultramicroscopy 2017;173. https://doi.org/10.1016/j.ultramic.2016.11.013.

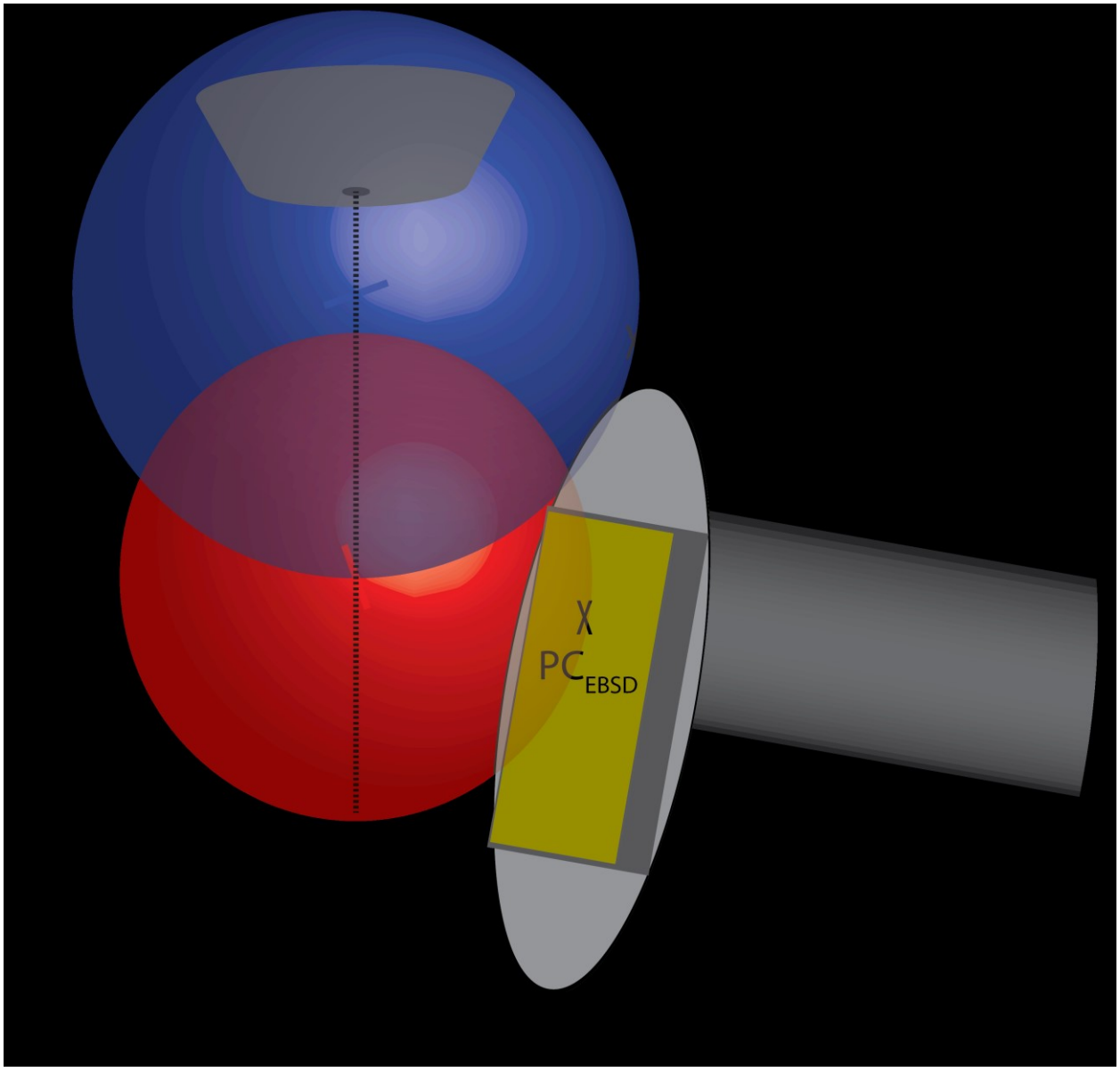

Figure 1. Schematic representation of the effect of working distance used in TKD and EBSD experiments on scattering geometries with the respective locations of the PCs, as well as the different radii of the Ewald's sphere for the EBSD and TKD experimental settings.

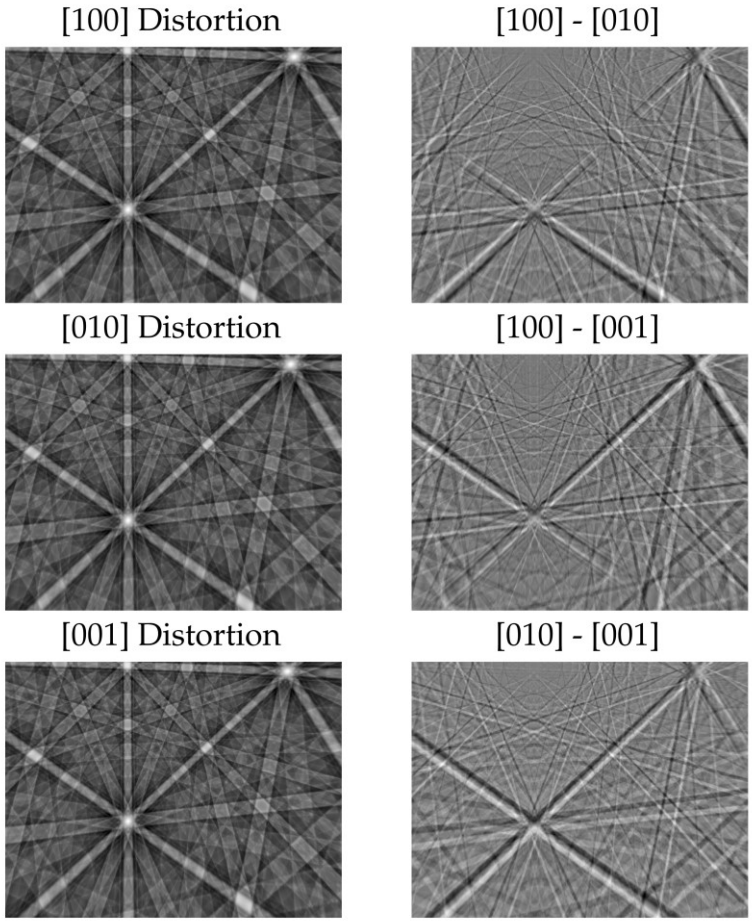

Figure 2. Comparison of the simulated EDP for the EBSD geometry for a tetragonal distortion along the [100], [010], and [001] directions. Difference maps between EDP for a, b, and c axis distortions highlight how these distortions impact different regions of the EDP.

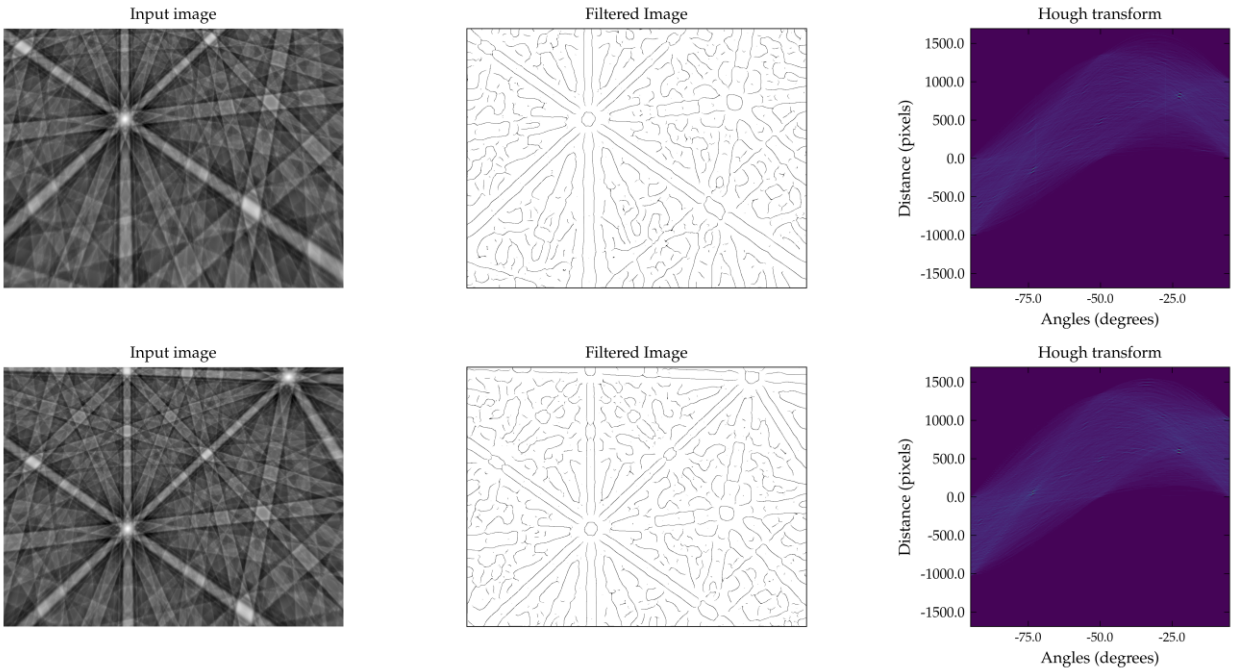

Figure 3. Comparison of the simulated EBSD pattern and Hough transform steps for the TKD (top) and EBSD (bottom) geometries. The gnomonic projections are evidenced by an increase in the widths and non-linearity of Kikuchi lines in the EDPs.

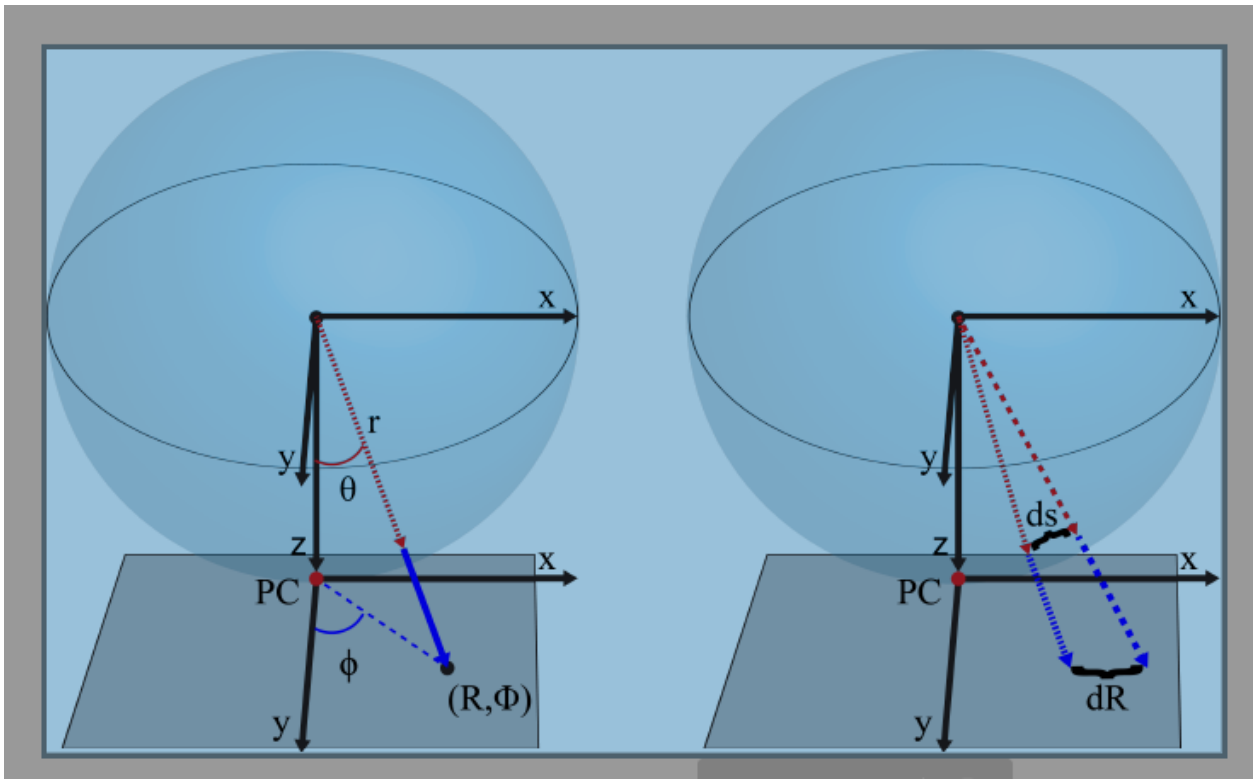

Figure 4. Illustration of the gnomonic projection present in EBSD and TKD for (Left) the projection of a point on the diffraction sphere is onto the plane of the detector and (Right) how a small angular perturbation (dθ) affects the position on the diffraction sphere (ds) and projection onto the detector (dR).

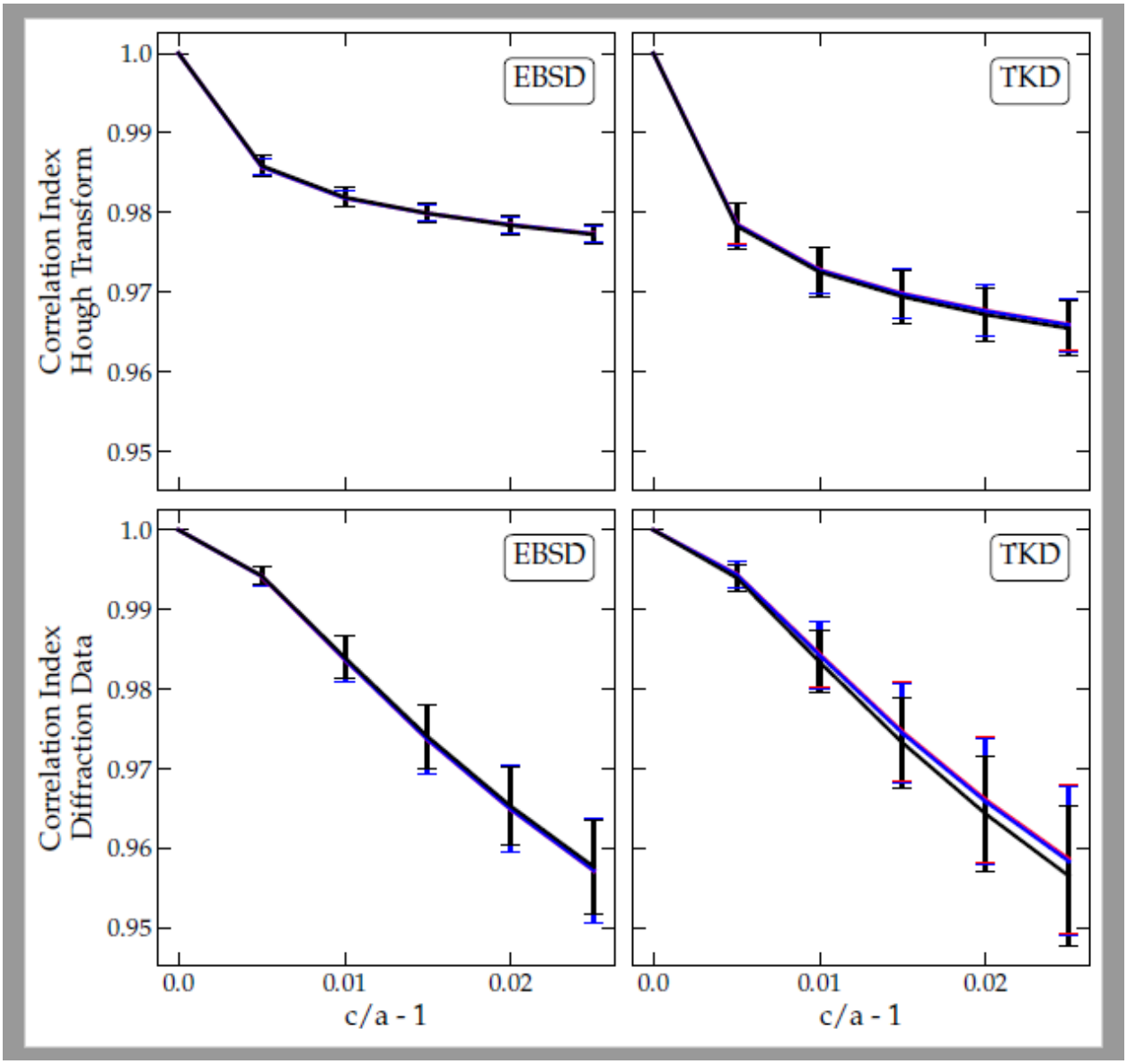

Figure 5. Normalized inner-product of the EBSD/TKD data for tetragonally distorted Al unit cell oriented 90 degrees apart in Hough space (top) and diffraction space (bottom). Error bars represent the 95% confidence interval determined from the standard deviation in results for all datasets.

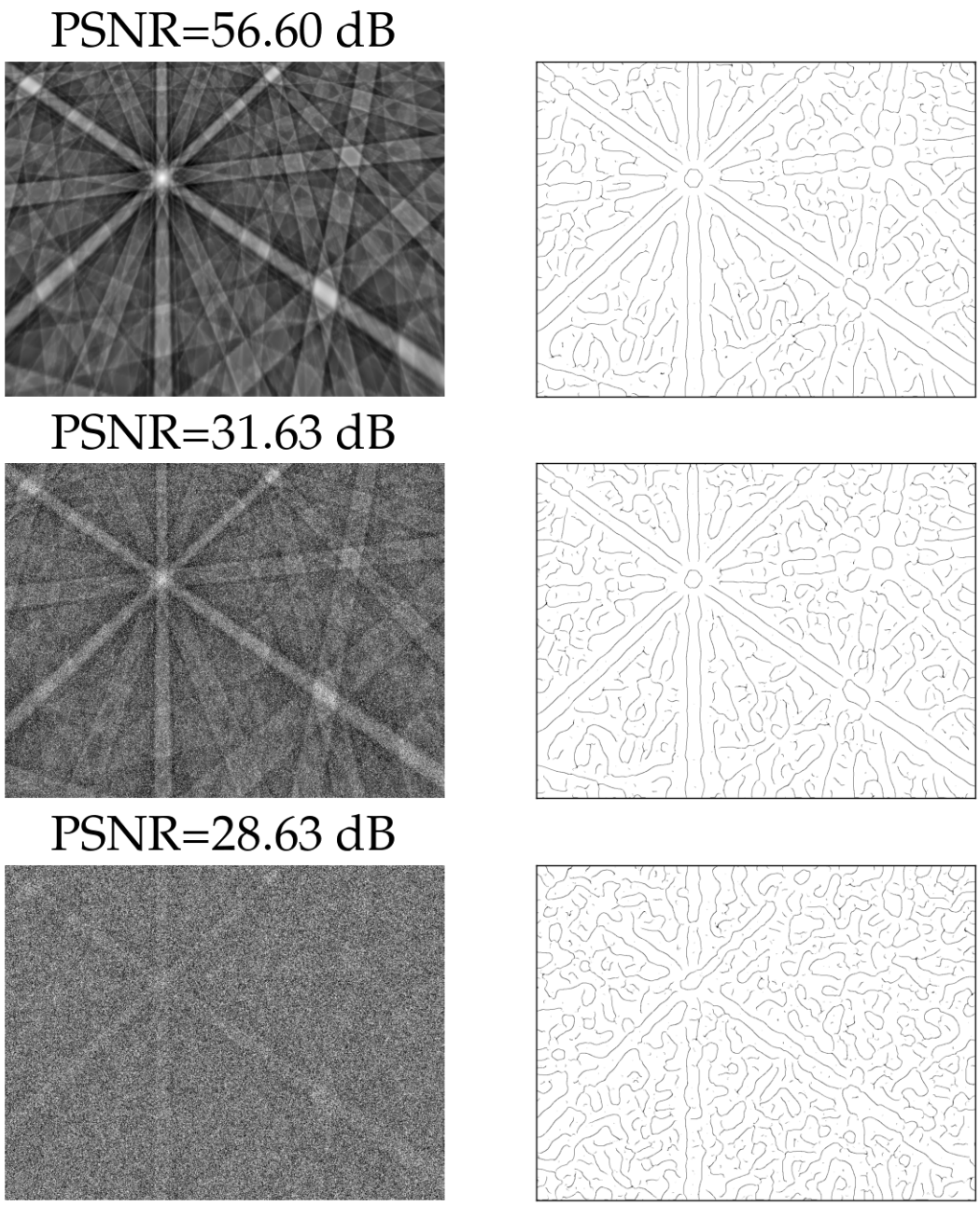

Figure 6. Impact on the level of noise impacts the quality of the Hough transform. The highest noise (lowest PSNR) still captures significant features in the data. However, these data are corrupted with randomness associated with the lower signal-to-noise data.

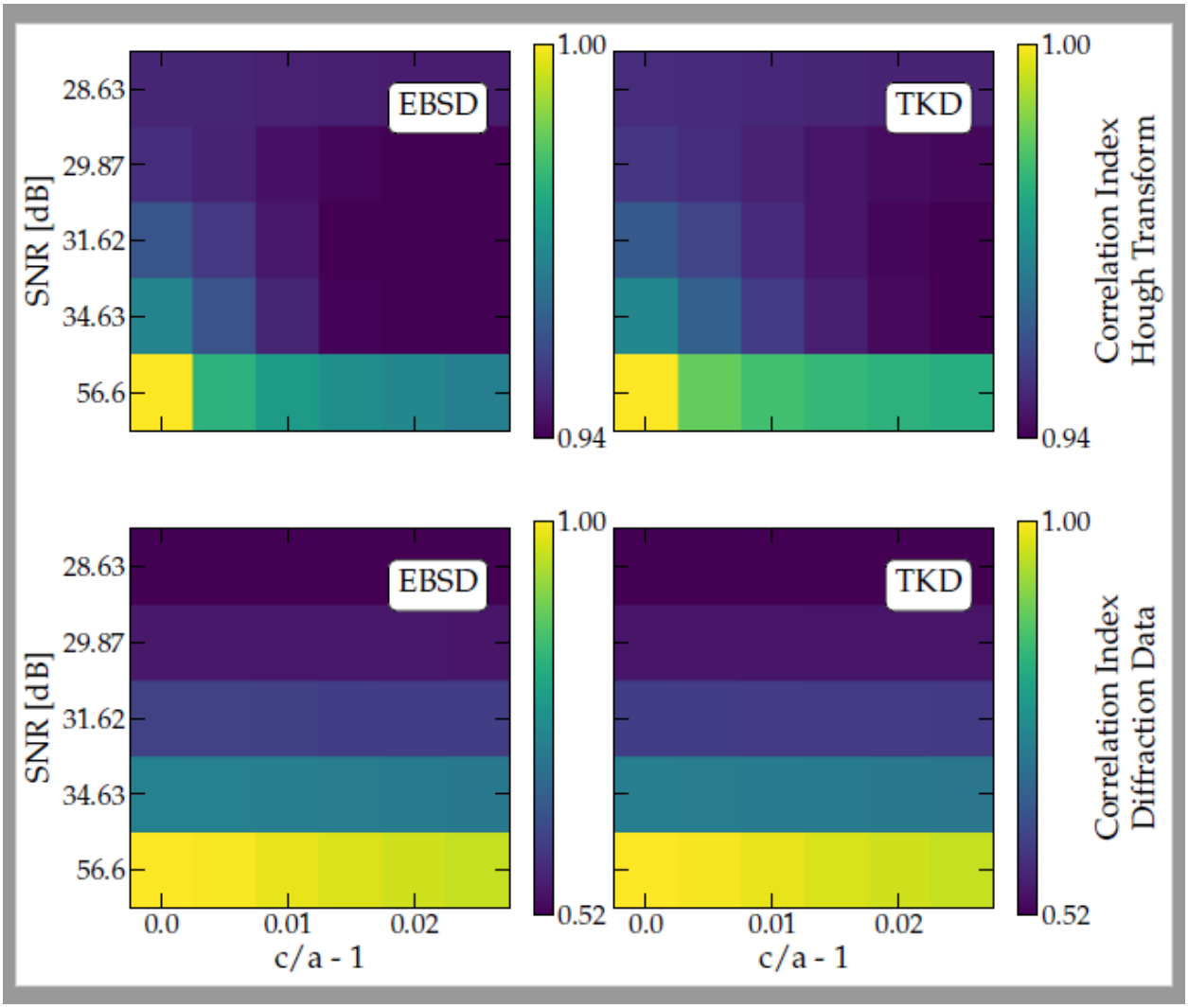

Figure 7. Lattice distortions-dependent correlation index for data simulated with varying levels of noise. The differences in the magnitude of the correlation index are related to how noise impacts different spaces where the normalized inner-product is performed.